AGU PUBLICATIONS

JGR

Journal of Geophysical Research: Space Physics

RESEARCH ARTICLE
10.1002/2016JA023656

The evolution of solar wind strahl with heliospheric distance

G. A. Graham[1], I. J. Rae[1], C. J. Owen[1], A. P. Walsh[2], C. S. Arridge[3], L. Gilbert[1], G. R. Lewis[1], G. H. Jones[1], C. Forsyth[1], A. J. Coates[1], and J. H. Waite[4]

[1]Department of Space and Climate Physics, Mullard Space Science Laboratory, University College London, Dorking, Surrey, UK, [2]European Space Astronomy Centre, Urb. Villafranca del Castillo, Spain, [3]Department of Physics, Lancaster University, Bailrigg, UK, [4]Southwest Research Institute, San Antonio, Texas, USA

Key Points:
- Using Cassini we study the evolution of strahl pitch angle widths with energy across 1 to 5.5 AU
- In general, strahl pitch angle widths broaden at an approximately constant rate for most energies
- We conclude strahl is most likely scattered to form part of the halo at large heliospheric distances

Correspondence to:
G. A. Graham,
georgina.graham@ucl.ac.uk

Citation:
Graham, G. A., et al. (2017), The evolution of solar wind strahl with heliospheric distance, *J. Geophys. Res. Space Physics*, *122*, 3858–3874, doi:10.1002/2016JA023656.

Received 4 NOV 2016
Accepted 11 MAR 2017
Accepted article online 17 MAR 2017
Published online 12 APR 2017

Abstract Field-aligned beams of suprathermal electrons, known as "strahl," are a frequently observed constituent of solar wind plasma. However, the formation and interplanetary evolution of the strahl electron populations has yet to be fully understood. As strahl electrons travel away from the Sun, they move into regions of decreasing magnetic field strength and thus are subject to adiabatic focusing. However, the widths of strahl pitch angle distributions observed at 1 AU are significantly broader than expected. Previous investigations have found that the average observed strahl pitch angle width actually increases with heliocentric radial distance. This implies that strahl electrons must be subjected to some form of pitch angle scattering process or processes, details of which as of yet remain elusive. In this paper, we use Cassini electron measurements to examine strahl beams across a distance range of approximately 8 AU, from its Earth Flyby in 1999 until its insertion into orbit around Saturn in 2004. We find that, in general, there is a relatively constant rate of broadening of strahl pitch angle distributions with distance between ~ 1 and 5.5 AU. Our results from beyond this distance indicate that the strahl population is likely to be completely scattered, presumably to form part of the halo. We find multiple energy dependences at different radial distances implying that there are multiple strahl scattering mechanisms in operation.

1. Introduction

Decades of observations show that solar wind electron velocity distributions at ~1 AU are made up of three major constituents: one thermal (<50 eV) population referred to as the "core;" and two suprathermal (~70–1000 eV) electron populations known as "halo" and "strahl" [e.g., *Feldman et al.*, 1975; *Lin*, 1998; *Maksimovic et al.*, 2005; *de Koning et al.*, 2006]. The nature of these populations is illustrated in Figure 1. Although anisotropies are common in the solar wind, the core and halo populations are generally observed to be relatively isotropic compared to the strahl, which is composed of a strongly field-aligned beam of electrons. Strahl electrons travel away from the Sun, along interplanetary magnetic field (IMF) lines and can be observed in either the parallel or antiparallel magnetic field direction [e.g., *Feldman et al.*, 1978; *Pilipp et al.*, 1987a] or indeed both directions in certain circumstances [e.g., *Gosling et al.*, 1987].

Suprathermal electrons are thought to originate in the solar corona [e.g., *Viñas et al.*, 2000; *Štverák et al.*, 2008; *Che and Goldstein*, 2014]. A number of mechanisms are invoked to explain the election populations' formation within the corona and existence within the solar wind and hence a firm consensus on their origin has yet to be reached. Theoretical investigations into the evolution of electrons in the solar corona and solar wind have shown that the formation of a suprathermal electron beam is due strong magnetic focusing effects [e.g., *Pierrard et al.*, 2001; *Smith et al.*, 2012; *Landi et al.*, 2012]. The presence of an near-isotropic halo population in the solar wind at 1 AU is then frequently explained by scattering of suprathermal electrons via wave-particle interactions or by global reflection in the heliosphere [e.g., *Smith et al.*, 2012; *Landi et al.*, 2012]. However, a recent investigation by *Che and Goldstein* [2014] into the effect of nanoflare acceleration on electron evolution found that a core-halo feature could form before a strahl beam in the low corona near sector boundaries. Moreover, Coulomb collisions were found to be insufficient to thermalize the distribution before the plasma is advected into the solar wind. *Che and Goldstein* [2014] then suggest that although the halo could form in the inner corona, some form of scattering is still required to counter adiabatic focussing and preserve the halo population at larger radial distances. In order understand the processes surrounding the coronal origins of suprathermals, it is necessary to first determine what processes affect the electrons on their journey away from the Sun and thus to examine their evolution as they propagate outward through the heliosphere.

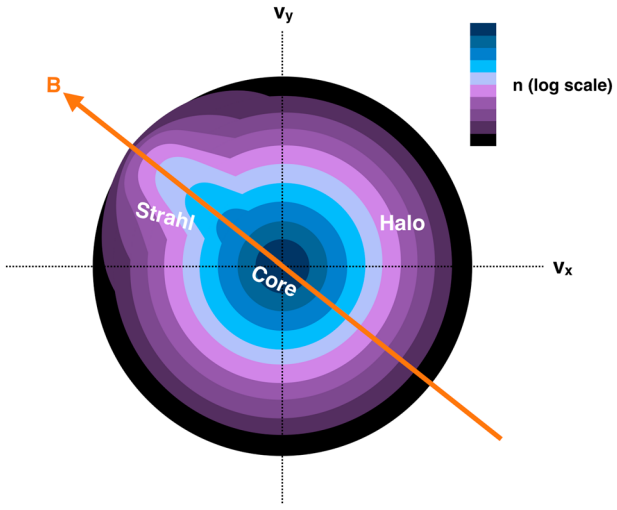

Figure 1. An illustration of an typical solar wind electron 2-D velocity distribution. The figure shows the electron number density (n) as a function of velocity (v_x and v_y). The direction of the magnetic field (**B**) lying in this plane is shown by the orange arrow. The isotropic, relatively cool, and dense population shown at the center of the distribution is known as the core. The less-dense, relatively isotropic, suprathermal population that extends out to higher velocities is known as the halo. The strongly field-aligned beam of electrons observed at suprathermal energies (velocities) is known as the strahl.

The majority of solar wind heat flux is transported by the outflow of suprathermal electrons traveling away from the Sun, into interplanetary space [e.g., *Feldman et al.*, 1975; *Scime et al.*, 1994]. This is despite the much lower relative number density of the suprathermal populations (~5% at 1 AU) as compared to the thermal core [*Feldman et al.*, 1975]. Recent investigations have shown that the heat flux is closely related to the relative drift between the core and the halo populations [*Bale et al.*, 2013], which may be the relic of an electron two stream instability that develops in the low corona [*Che and Goldstein*, 2014]. It has also been shown that when a clear strahl beam is observed, the majority of solar wind heat flux is carried by the strahl electrons [*Pilipp et al.*, 1987a]. Hence, strahl behavior could provide insight into the mechanisms related to the evolution of solar wind heat flux.

Strahl is, by definition, strongly field-aligned, and its constituent electrons have a high velocity relative to the bulk plasma flow. As a consequence, strahl electrons travel at high relative speeds along the Parker spiral field. Hence, understanding unidirectional and bidirectional strahl trajectories can be used to determine large-scale IMF topology and provide near-instantaneous indications of solar connectivity [e.g., *Pilipp et al.*, 1987b; *Owens et al.*, 2008]. Bidirectional strahl are thought to be good indicators of newly formed magnetic loops and have also been observed when suprathermal electrons are reflected at interplanetary shocks [e.g., *Gosling et al.*, 1987; *Owens and Forsyth*, 2013]. It has also been suggested that bidirectional electron heat flux events are one of the more consistent signatures of coronal mass ejections, particularly at 1 AU [e.g., *Gosling et al.*, 1987]. More recently, the key role strahl pitch angle distributions can play in the determination of IMF global topology was illustrated in a study by *Li et al.* [2016], which used predictions of suprathermal pitch angle distributions to test the validity of a proposed IMF mapping technique.

1.1. Radial Evolution of Strahl

It is generally accepted that the strahl population consists of electrons with energies large enough to escape the electrostatic potential of the Sun [*Pierrard et al.*, 2001]. Once outside the Sun's potential well, the electron collision frequency is reduced to a level that, in principle, allows both electron energy and magnetic moment to be conserved [*Hammond et al.*, 1996]. Electrons traveling outward into regions of decreasing magnetic field strength should therefore experience strong adiabatic focussing, resulting in the formation of a highly field-aligned electron population [*Owens and Forsyth*, 2013]. Indeed, it has been shown that strong adiabatic focussing can produce a clear strahl signature in the electron distribution function within as little as 10 solar radii, when constrained by typical coronal hole conditions [*Smith et al.*, 2012]. It thus follows that in the absence of other influences, the strahl beam should continue to narrow with heliocentric distance and become highly collimated within ~ 0.5 AU [*Owens et al.*, 2008]. However, strahl beams observed in the near-Earth solar wind have been shown to have a pitch angle width that is larger than predicted for adiabatic focussing to be the sole effect experienced by the strahl, with a range of at least 5–90° [*Anderson et al.*, 2012]. This implies that strahl electrons must be subject to some form of scattering process as they travel outward from the Sun.

The majority of strahl studies have been based upon observations close to 1 AU. However, there are two key results regarding strahl evolution over heliocentric distances large enough to observe radial trends. First, average strahl pitch angle width increases with radial distance from ~ 1 to 2.5 AU [*Hammond et al.*, 1996]. Second, the strahl population has been observed to decrease relative to the halo population with heliospheric distance

[e.g., *Maksimovic et al.*, 2005; *Štverák et al.*, 2009]. These results imply that strahl electrons are scattered as they travel outward away from the Sun, until eventually they form part of the diffuse halo population. These statistical trends are supported by direct observations of intense scattering of strahl electrons to form a proto-halo population at 1 AU [*Gurgiolo et al.*, 2012].

Solar wind plasma is too tenuous for Coulomb collisions to produce the scattering effect necessary to match suprathermal electron observations [e.g., *Hammond et al.*, 1996; *Vocks et al.*, 2005]. At 1 AU the mean free path is comparable with the typical length scales of the system [*Štverák et al.*, 2008]. As a consequence, numerous investigations have concluded that the strahl scattering mechanism(s) must involve electron interaction with plasma waves rather than via collisions [e.g., *Saito and Gary*, 2007; *Pagel et al.*, 2007]. The exact nature of the scattering process or processes remains elusive, but previous studies invoke an interaction with whistler mode waves as being primarily responsible [e.g., *de Koning et al.*, 2006; *Pagel et al.*, 2007; *Anderson et al.*, 2012]. It should also be noted that it is not known whether these scattering processes operate continuously or intermittently throughout the heliosphere.

The nature and heliospheric locations/conditions of the strahl scattering process(es) have significant implications for the applicability of strahl trajectories as tool for inferring IMF topology. For example, the bidirectional signature associated with IMF loops may often be scattered to the extent that is lost [e.g., *Hammond et al.*, 1996; *Maksimovic et al.*, 2005; *Owens et al.*, 2008]. This is particularly relevant for the sunward component of bidirectional strahl as it is traveling into regions or increasing magnetic field strength and therefore will experience broadening due to conservation of magnetic moment. Establishing the bounds of their utility for IMF topology determination through further investigation into the radial variability of strahl signatures is therefore highly desirable.

1.2. Energy Dependence of Strahl Pitch Angle Width

In order to ascertain the nature of the strahl scattering mechanism(s), it is necessary to understand pertinent energy relations, particularly if resonant wave-particle interactions play an important role. There are multiple different and seemingly contradictory findings with regard to the variation of strahl pitch angle width as a function of electron energy. It has been shown that at a fixed radial distance:

1. Strahl pitch angle width decreases with increasing electron energy [e.g., *Feldman et al.*, 1978; *Pilipp et al.*, 1987a; *Fitzenreiter et al.*, 1998].
2. Strahl pitch angle width increases with increasing energy [*Pagel et al.*, 2007].
3. At a given time, it is equally probable that strahl width could increase or decrease with increasing electron energy [*Anderson et al.*, 2012].
4. There is no strong correlation between strahl width and electron energy [*Hammond et al.*, 1996].
5. Strahl pitch angle distributions are narrower in the fast solar wind than the slow solar wind but both types of solar wind display the same energy relation, which is strahl pitch angle width decreasing with increasing electron energy [*Fitzenreiter et al.*, 1998].
6. Proximity to interplanetary magnetic field (IMF) sector boundaries results in strahl pitch angle distribution broadening that is independent of electron energy [*Pilipp et al.*, 1987b].

For distances beyond 1 AU, it has been shown that the increase in strahl pitch angle width with radial distance is energy dependant and that low-energy electrons display greater broadening per astronomical unit than higher energies [*Hammond et al.*, 1996]. The above results make it apparent that there is no clear consensus regarding the strahl pitch angle scattering mechanism, as there is no clear consensus on strahl behavior. It should be noted that the results obtained in the *Hammond et al.* [1996] study were derived from Ulysses observations over a wide range of heliospheric latitudes as well as radial distances, and that there were indications that latitude variations may have some effect on strahl pitch angle distributions.

The different energy relations previously reported suggest that multiple scattering mechanisms may be present in the solar wind. However, it is unknown whether there is a scattering mechanism that plays a dominant role in the evolution of strahl, or indeed, whether the scattering is a continuous process or intermittently occurring when conditions in the solar wind are favorable. Accordingly, a variety of resonant and non-resonant wave-particle interactions have been proposed to be responsible. However, whistler mode waves are often proposed as the most likely scattering mechanism [e.g., *Fitzenreiter et al.*, 1998; *Hammond et al.*, 1996; *de Koning et al.*, 2006; *Anderson et al.*, 2012]. This is supported by multiple spacecraft observations of

whistler-like fluctuations in the solar wind, such as the statistical study by *Lacombe et al.* [2014] which found right-handed, circularly polarized, quasi-parallel fluctuations in ~ 10% of solar wind data. Whistler mode waves are also an appealing solution to these seemingly contradictory energy dependence observations, as whistler mode scattering due to resonant interaction with electrons has been theorized to result in different strahl width versus energy relations, depending on the source of the whistler fluctuations [*Saito and Gary*, 2007, and references therein]. It has been proposed that a broadband whistler spectrum resulting from turbulent cascade could produce strahl with a beam width which increases with strahl energy [*Saito and Gary*, 2007]. Conversely, the same study proposed that a core electron temperature anisotropy ($T_{\perp}/T_{\parallel} > 1$) would lead to excitation of the whistler anisotropy instability and thereby producing enhanced whistler fluctuations that result in strahl width which decreases with strahl energy.

1.3. Motivation for This Study

It has been shown by *Owens et al.* [2008] that in the presence of a constant scattering rate, independent of time, heliocentric distance, and electron energy, the geometric effect of a Parker spiral IMF can, to a certain extent, explain why adiabatic focussing dominates closer to the Sun (within ~ 20 R_s), whereas at larger heliocentric distances pitch angle scattering becomes more influential. This is because the Parker spiral IMF becomes less radial at distances further from the Sun and so for a given unit of time/unit distance along an IMF line, a field-aligned electron further away from the Sun experiences a smaller decrease in magnetic field strength but the same constant scattering rate. It has also been shown by *Owens et al.* [2008] that that time-of-flight effects could account for some of the apparent energy dependence of strahl pitch angle distribution broadening described. As electrons with greater velocities travel further along an IMF line in a given unit of time and therefore experience a larger decrease in magnetic field strength and greater adiabatic focussing effects [*Owens et al.*, 2008]. This study also suggested that this effect should decrease with increasing heliolatitude, as the Parker IMF becomes less tightly wound.

Indications of strahl electrons have been found as far out at ~10 AU by *Walsh et al.* [2013] using the Cassini spacecraft. *Walsh et al.* [2013] found that the estimated strahl pitch angle width was narrower than predicted by extrapolation of previous observations from within 2.5 AU. Hence, it was concluded that the rate of scattering must decrease with increasing radial distance. It was also suggested that this finding was consistent with whistler mode wave interaction as the primary strahl pitch angle scattering mechanism, since the effectiveness of whistler mode scattering depends on the available wave power below the electron gyrofrequency, and both wave power and the electron gyrofrequency decrease with radial distance [*Hu et al.*, 1999; *Vocks et al.*, 2005].

Given the contradictions and open questions discussed above, a consistent measurement of suprathermal electron distributions across a wide range of heliospheric distances is needed in order to resolve these ambiguities. In this paper, we use Cassini electron spectrometer and magnetometer cruise phase and flyby data, from ~1 to 9 AU, in order to investigate the radial evolution of strahl near the equatorial plane of the heliosphere. By using data from the same instrument across a radial distance range of 8 AU, we are able to extend previous studies of strahl evolution without the additional complications of cross-calibrating multiple spacecraft data sets. Moreover, by using the Cassini mission in particular, we are able to avoid any possible heliospheric latitudinal dependencies on strahl evolution. In this way, we link the numerous previous studies of strahl made within 4 AU with those of *Walsh et al.* [2013] and investigate whether the indications of strahl at 10 AU are indeed statistically likely.

2. Instrumentation

The Cassini-Huygens mission to explore the Kronian System began on 15 October 1997 when the spacecraft was launched from Cape Canaveral, Florida. Cassini entered its first orbit around Saturn approximately 7 years later on 1 July 2004, after traveling a distance of 3×10^9 km [*Matson et al.*, 2003]. Figure 2 shows the spacecraft trajectory from launch to the end of 2004. During its interplanetary journey, the Cassini spacecraft performed both Earth and Jupiter flybys, during which scientific data from the Cassini Plasma Spectrometer (CAPS) [*Young et al.*, 1998] and the dual-technique magnetometer (MAG) [*Dougherty et al.*, 2004] were obtained. There are also intervals during the cruise phases between planetary observations during which CAPS and MAG were both acquiring data. This is illustrated in Figure 2, which show the Cassini interplanetary trajectory projected onto the heliocentric inertial *x-y* plane. Sections marked in red show where the data necessary to conduct

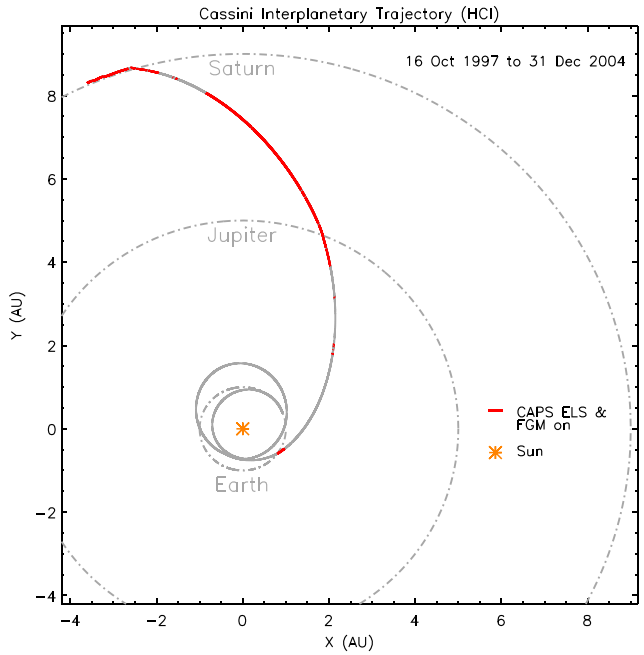

Figure 2. The trajectory of Cassini en route to Saturn from 16 October 1997 to 31 December 2004, as projected onto the Heliocentric Inertial (HCI) *X-Y* plane. The red line represents sections where and both CAPS ELS and MAG FGM were collecting data. The Sun is represented by a orange star, and the approximate orbits for Earth, Jupiter, and Saturn are shown by grey dash-dotted lines. The Earth flyby (closest approach) took place on 18 August 1999, the Jupiter flyby (closest approach) took place on 30 December 2000, and the Saturn orbit insertion took place on 01 July 2004.

this study were available. This study uses data from CAPS electron spectrometer (ELS) and MAG, obtained as Cassini traveled to Saturn, in order to achieve a large heliocentric radial range of ~1–9 AU, while remaining in the ecliptic plane.

Electron measurements are provided by the ELS sensor for CAPS, which is a hemispherical top hat electrostatic analyzer [*Young et al.*, 1998]. CAPS ELS has an energy/charge response range of ~0.5–27,000 eV/*e* is composed of eight anodes, providing an instantaneous field of view (FOV) of 5.2° in the azimuthal direction and ±80° in elevation (20° per anode) [*Linder et al.*, 1998]. The ELS is mounted with the other CAPS sensors, on a rotating platform driven by a motor actuator, that is able to sweep through ~200° in the ELS azimuthal direction in approximately 3 min [*Young et al.*, 2004]. Although, it should be noted that this is the maximum actuation range and it is not always implemented. The ELS has a cadence of 2 s and 63 energy bins; however, the time and/or energy resolution of the data were sometimes reduced by summing over several energy sweeps and/or pairing energy bins if CAPS ELS was assigned low telemetry priority [*Young et al.*, 2004; *Arridge et al.*, 2009]. For example, during the Earth flyby, the actuator only sweeps through 120° and the temporal cadence was limited to ~10 s [*Rymer et al.*, 2001]. It should also be noted that other instruments on board the Cassini spacecraft intrude upon the CAPS ELS FOV (see *Young et al.* [2004], for more details) and that when using CAPS ELS data, the background count rate resulting from Cassini's radiation sources must also be accounted for (see *Arridge et al.* [2009], for more details). In order to determine electron pitch angle distributions, the ELS observations are related to the concurrent magnetic field direction. Measurements are provided by the fluxgate magnetometer (FGM) for MAG [*Dougherty et al.*, 2004]. The FGM is mounted midway along the 11 m magnetometer boom, and we use 1 s cadence data throughout this study.

3. Method

3.1. Determining Suitable Periods for Strahl Pitch Angle Width Observations

Reliable measurement of strahl beam width requires that two key criteria are fulfilled. First, the observations were made while Cassini was in the "pure" solar wind. Second, the selected suprathermal electron pitch angle distributions must cover the full range of 0–180°, such that strahl can be clearly resolved. The first condition was fulfilled by removing times when Cassini is behind a planetary bow shock from the data set.

For details of when Cassini was not in the solar wind we refer the reader to *Rymer* [2004], *Arridge et al.* [2006], and *Achilleos et al.* [2006]. An outline of how the second requirement was achieved from available observations is described below.

As established in section 2 the ELS FOV coverage is variable. This means that for one energy sweep, or even one actuation, the observed electron distribution may not always contain the full electron pitch angle range required to determine the characteristics of the strahl component. Therefore, in order to assemble full and representative 180° pitch angle distributions using CAPS ELS, we identified individual parcels of relatively consistent solar wind, in which the CAPS ELS sensor has sufficient time to sample the full pitch angle distribution, while the plasma parameters remain comparatively steady.

It has been suggested [*Borovsky*, 2008] that the solar wind is made up of a network of entangled magnetic "flux tubes," each containing a distinct solar wind plasma population, and that these flux tubes are fossil structures originating from the solar corona. In this scenario, there should be limited changes in the plasma properties or behavior within a particular flux tube. Hence, the electron data recorded between the flux tube boundaries should be suitable for averaging over the longer periods of time required to obtain a distribution which covers the full pitch angle range. This approach is a means of minimizing the potential aliasing of the measured properties of two or more distinct plasma populations.

Borovsky [2008] showed that detection of large changes in the magnetic field direction and/or solar wind velocity can be used as a method for determining spacecraft crossing of a flux tube wall. However, due to limitations of the FOV outlined above, it is not always possible to determine the solar wind bulk parameters using Cassini CAPS. Thus, in order to perform our study of strahl over large heliospheric distances, we simply apply the magnetic criterion described in *Borovsky* [2008] to identify periods in which we might expect relatively steady electron populations. *Neugebauer and Giacalone* [2015] suggested that magnetic field magnitude changes are associated with tangential discontinuities more likely to originate in solar corona and therefore be associated with flux tube walls as opposed to rotational discontinuities that are associated with turbulence. Hence, we also implement an ancillary magnetic field magnitude criterion taken from *Neugebauer and Giacalone* [2015]. The criteria used in this study for flux tube wall determination based on changes in the magnetic field are as follows:

$$\Delta\theta = \cos^{-1}\left(\frac{\bar{\mathbf{B}}_{\text{inst}} \cdot \bar{\mathbf{B}}_{\text{av}}}{|\,\bar{\mathbf{B}}_{\text{inst}}\,||\,\bar{\mathbf{B}}_{\text{av}}\,|}\right) > 60° \tag{1}$$

$$\frac{|\,\bar{\mathbf{B}}_{\text{inst}} - \bar{\mathbf{B}}_{\text{av}}\,|}{|\,\bar{\mathbf{B}}_{\text{inst}}\,|} > 0.2 \tag{2}$$

where $\Delta\theta$ is the angular change in the magnetic field vector, $\bar{\mathbf{B}}_{\text{inst}}$ is the instantaneous 1 s resolution magnetic field vector, and $\bar{\mathbf{B}}_{\text{av}}$ is the calculated running average for the time period required for the actuator to sweep through ~180°.

3.2. Strahl Pitch Angle Observations Within a Solar Wind "Flux Tube"

The adapted flux tube criteria specified above were used to identify solar wind flux tube boundaries observed by Cassini for all time periods where both MAG and ELS data were available during its interplanetary journey (Figure 2). We then subtract the look direction and time-dependent background level count rate from the ELS data within each flux tube [*Arridge et al.*, 2009] and remove the data from obstructed parts of the FOV [*Walsh et al.*, 2013]. No spacecraft potential information is available, and so no photoelectron contamination correction was made to the data. However, photoelectron contamination is unlikely at suprathermal energies, and so this is not expected to affect our results [*Walsh et al.*, 2013]. For each ELS measurement we determine the pitch angle of the center of each anode based on the orientation of the anode relative to the magnetic field direction. These count rate measurements are then averaged into 10° wide pitch angle bins within each flux tube over the given time period detailed below. In order to achieve reasonable counting statistics while maintaining acceptable errors, the ELS data within each 10° pitch angle bin was subjected to a count rate criterion; all pitch angle bins must contain a sufficient number of individual count rate observations to produce an error for the mean count rate observation of $\leqslant 10\%$. We calculate the percentage propagated error ($\sigma_{\%\,\text{prop}}$) for the mean count rate for each bin as follows,

$$\sigma_{\%\,\text{prop}} = \frac{1}{m}\sqrt{\sum_{m=1}\left(\frac{\sigma}{x}\right)^2} \tag{3}$$

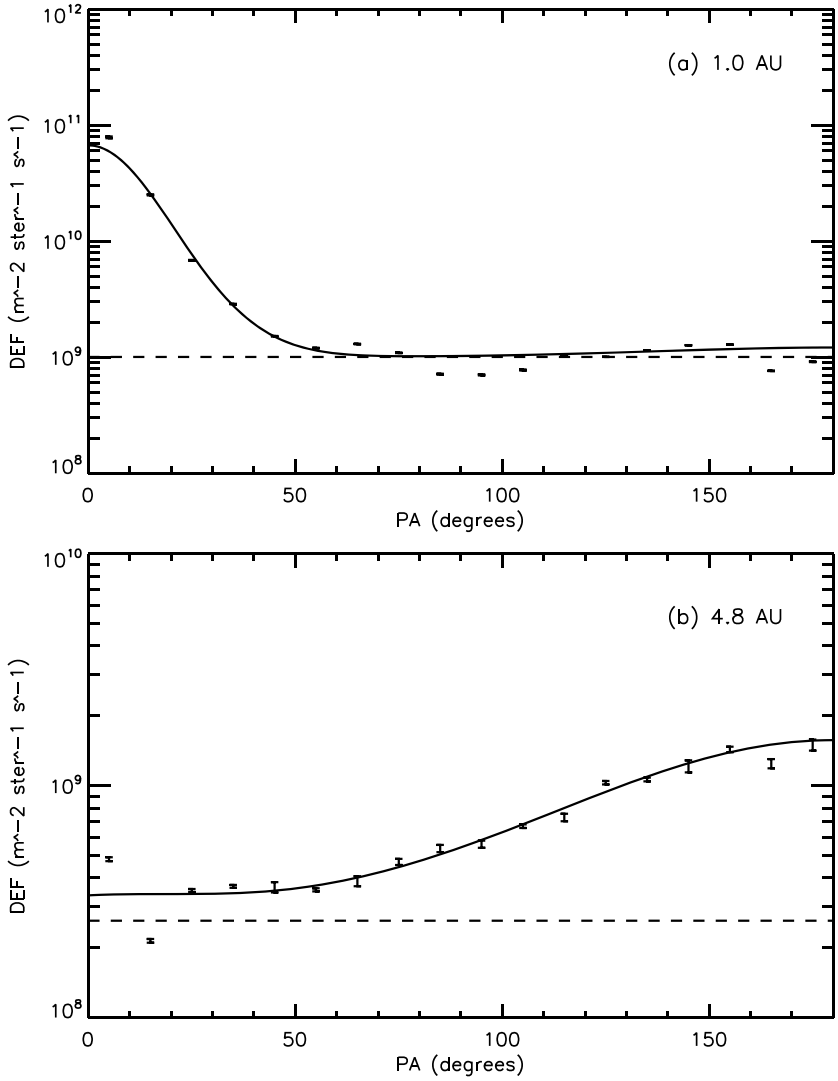

Figure 3. Electron pitch angle distribution observed at a heliocentric radial distance of (a) 1.0 AU and (b) 4.8 AU, plotted in units of eV m^{-2} sr^{-1} s^{-1} eV^{-1} (differential energy flux), for the CAPS ELS energy bin with central energy of 235.0 eV. Each data point represents the mean DEF determined for a 10° pitch angle bin. The solid line is a double Gaussian (one centered at 0° pitch angle and the other at 180°) plus a constant background term, fitted to the data using a non-linear least squares fit method [*Markwardt*, 2009]

where m is the number of observations, x is measured count rate, and σ is the count rate error (equivalent to the Poisson error on the count rate). The required number of observations (m_{req}) for each 10° pitch angle bin is therefore given by,

$$m_{req} = 10 \sqrt{\sum_{m=1} \left(\frac{\sigma}{x}\right)^2} \quad (4)$$

In this way, we are able to determine the shortest periods of data accumulation within a flux tube which are able to satisfy the criterion and we are able to average individual observations within these periods to produce as many statistically valid pitch angle distributions within a flux tube and hence between 1 and 9 AU as the data set can support. It should be noted that if the entire time within the flux tube was not enough to satisfy this criterion, then data obtained within this flux tube was rejected from our analysis. Finally, data from periods with telemetry modes resulting in reduced time resolution of CAPS ELS were included, but no data was used from periods with reduced energy resolution, in order to maintain consistent energy bins.

For each individual event that satisfied the criterion above, fits to the differential energy flux as a function of pitch angle were made for each suprathermal electron energy bin. The function chosen for fitting consisted

of the sum of two Gaussians, one centered on 0° pitch angle and the other on 180°, and a constant background. The full width half maximum (FWHM) of each Gaussian peak was then used as a measure of the width of the parallel (0°), antiparallel (180°), or bistreaming strahl beam, while the constant term represents an isotropic halo population, a method which has been implemented in multiple previous studies [e.g., *Hammond et al.*, 1996; *Anderson et al.*, 2012]. It should be noted that this fitting method means that halo temperature anisotropies are not considered in this study. However, we also only examine results where the fitted peak flux in at least one of the Gaussians is a minimum of 2 times greater than that of the background [e.g., *Anderson et al.*, 2012]. Distributions with a FWHM > 180° are not considered to contain strahl beams, as the full pitch angle distribution range is 180°, and thus, larger values represent an almost isotropic distribution [e.g., *Hammond et al.*, 1996; *Anderson et al.*, 2012]. In the case where a bidirectional strahl is found using the fitting technique, the most intense strahl beam is chosen for use in our analysis. This choice is made as it is likely that broader strahl in a counterstreaming event has traveled either along the longer path of a closed IMF loop, along an IMF loop in the Sunward direction and therefore experienced adiabatic broadening, or has been reflected back off of an upstream shock [*Gosling et al.*, 1993]. Hence, for these reasons, we compare the more intense strahl beam in a counterstreaming event to those events with unidirectional strahl. It is possible that the strahl beams may have been exposed to different scattering regimes along the different legs of a closed IMF loop. Hence, a future investigation that solely examined the radial evolution of bidirectional strahl would be informative. However, this would be challenging due to the relatively low occurrence of bidirectional strahl which are generally observed ~ 10% of the time in the solar wind whereas a single strahl beam is observed ~ 65% of the time [*Anderson et al.*, 2012]. Two representative electron pitch angle distributions that fulfill our analysis criteria and demonstrate our fitting technique are shown in Figures 3a and 3b. Both example distributions are for the CAPS ELS energy bin with a central energy of 235.0 eV. Figure 3a shows field-aligned strahl observed at ~1.0 AU, and Figure 3b shows broader, anti-field-aligned strahl observed at ~4.8 AU.

4. Results

In order to characterize the evolution of strahl beam width with heliocentric radial distance, we applied the criteria specified in section 3 to all periods during Cassini's interplanetary journey for which both ELS and MAG data were available (Figure 2). Figure 4 shows the median strahl electron pitch angle width, and median absolute deviation, as a function of radial distance for CAPS ELS energy bins with central energies ranging from ~70 to 600 eV. The upper bound of this energy range is chosen as count rates for ELS were too low to construct statistically acceptable pitch angle distributions above ~600 eV, in particular at large radial distances. The lower energy bound was chosen to allow direct comparison with observations made in previous strahl investigations [e.g., *Hammond et al.*, 1996]. The median value is obtained from radial distance bins of 0.5 AU width and was chosen over the mean to reduce the influence of skewed data and/or statistical outliers.

Examination of Figure 4 shows that, in general, strahl width increases with radial distance from ~1 to 5.5 AU. This is in agreement with previous pitch angle width trends determined using Ulysses observations from ~1 to 2.5 AU [*Hammond et al.*, 1996]. However, it should be noted that many of our results diverge from a linear increase with radial distance after ~3 AU, with some energies, such as ~320 eV, displaying variable median pitch angle width and others, such as ~380 eV, displaying a more asymptotic trend. Most observations made beyond ~5.5 AU were not suitable for our analysis because they did not fulfill the measurement criteria outlined above (section 3.2). Therefore, the rate of pitch angle scattering beyond this distance remains unknown and we focus on the measurements within ~5.5 AU. It should also be noted that some radial distances have been omitted due to a lack of available data.

The variation of strahl beam width with electron energy for a given radial distance is shown in Figure 5. From top to bottom, Figure 5 presents the median strahl width as a function of electron energy for radial distances of 5.5, 5, 4.5, 3, and 1 AU, normalized to the maximum value observed at that radial distance. At both 1 and 4.5 AU two relatively clear energy relationships can be observed. For lower electron energies (~70–150 eV), there appears to be an inverse relationship between strahl width with electron energy, whereas for higher energies (~200–600 eV), strahl widths increase with electron energy. However, we note here that the computed uncertainties are large, and hence, we cannot make any quantitative conclusions on these relationships. The results obtained at 3 AU are less clear, although there is a sharp increase in strahl width observed for the lowest strahl energies (up to ~120 eV). Following that there is an approximately uniform strahl width with energy which may show signs of a slight peak at ~300 eV electrons. Slight peaks can also be seen in the results from

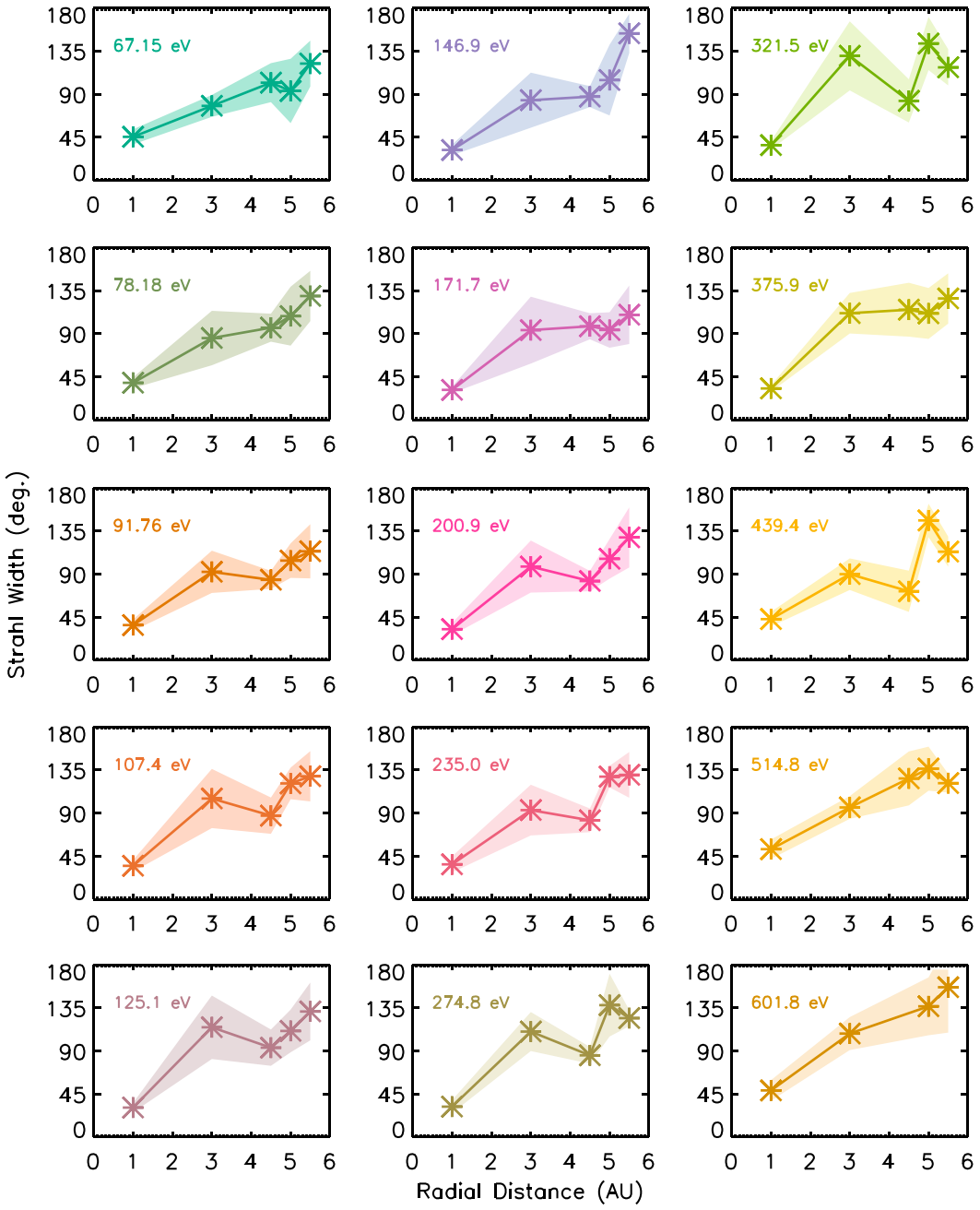

Figure 4. Strahl electron pitch angle width as a function of radial distance for CAPS ELS energy bins with central energies ranging from 67.15 to 601.8 eV. The plot shows median strahl width versus radial distance for 0.5 AU bins. The color-filled polygons represent the median absolute deviation.

5 AU, for ~100 eV electrons, although we note here again that the uncertainties in Figure 5 are quite large, and hence, these relationships are merely indicative. The results from 5.5 AU show an approximately uniform strahl width with energy.

Figure 6 shows a direct comparison of pitch angle width results for the common energy channels of Ulysses [*Hammond et al.*, 1996] and Cassini. The radial changes in strahl pitch angle width determined in our study were fitted by a linear function using a least squares fit method. Examination of the fits reveals that a linear increase in median strahl pitch angle with radial distance is appropriate for all compared energies. The rate of increase in strahl pitch angle width with radial distance, obtained using Ulysses observations, was found

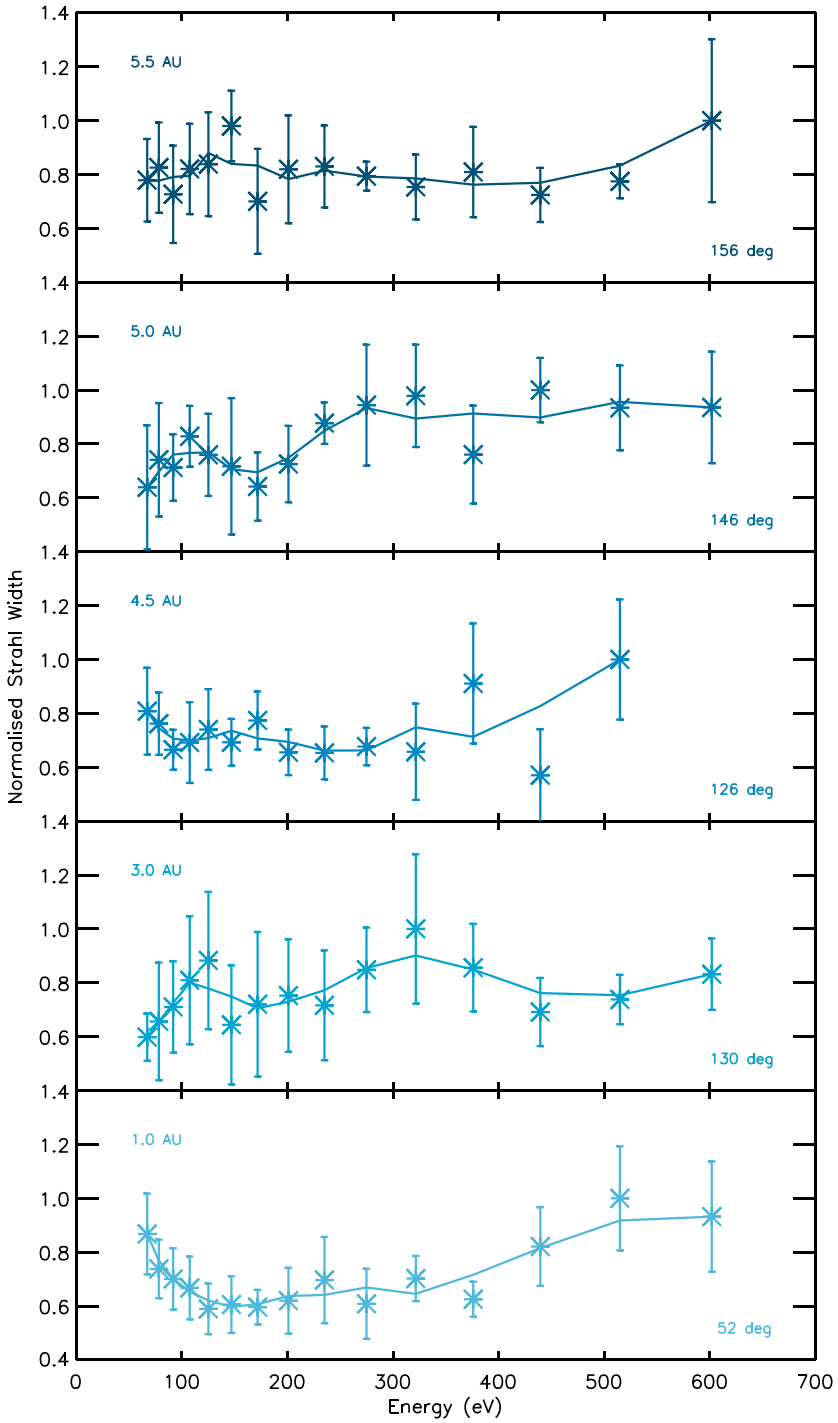

Figure 5. Strahl electron pitch angle width versus electron energy for (fifth panel) 1 AU to (first panel) 5 AU. The error bars plotted represent the median absolute deviation. The solid lines are a 3-point smooth of the data and are used only to highlight the trends observed. The values are normalized to the maximum strahl pitch angle width at each radial distance; the values of which are written in the bottom right of each panel.

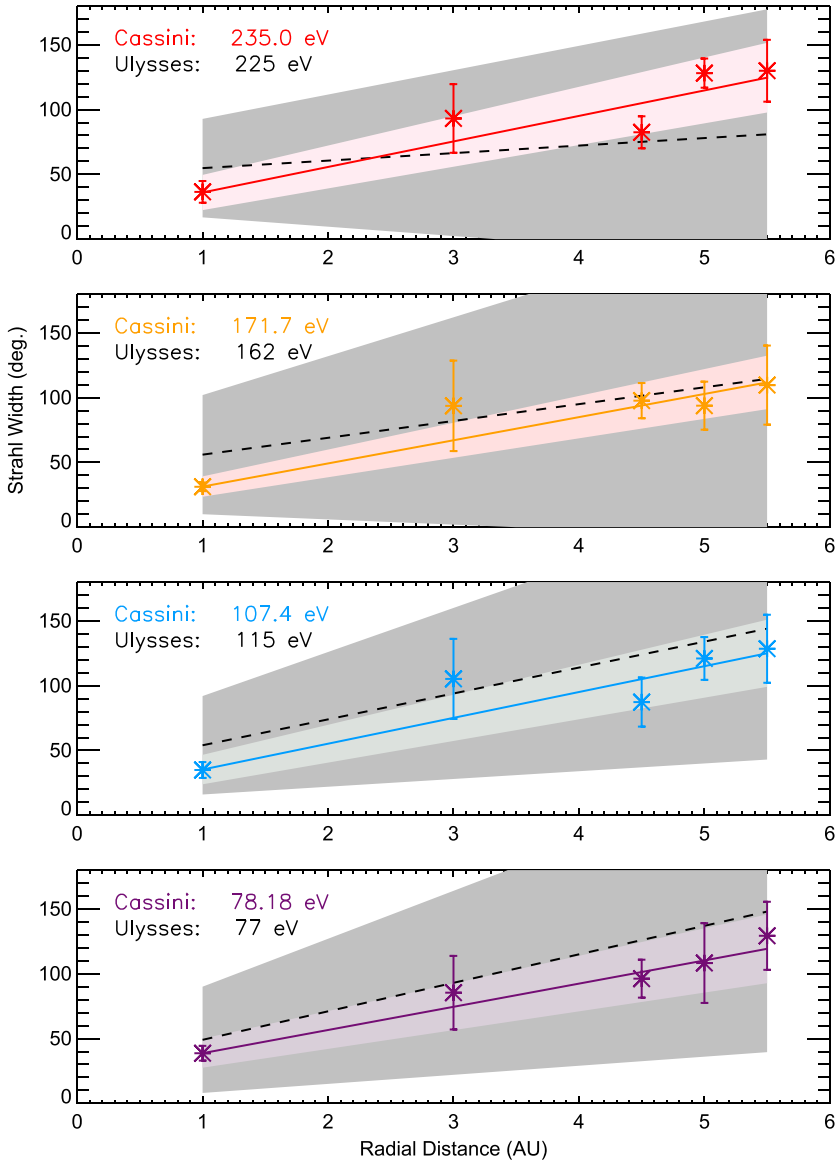

Figure 6. Strahl electron pitch angle width as a function of radial distance for CAPS ELS energy bins with central energies 78.18 (purple), 107.4 (blue), 171.7 (orange), and 235.0 eV (red). Each panel shows median strahl width versus radial distance for 0.5 AU bins. The error bars plotted represent the median absolute deviation; the solid lines are a linear fit to the results and the color-filled polygons show the 1σ errors for the linear fits. The dashed lines represent the extrapolated Ulysses results for 77, 115, 162, and 225 eV from *Hammond et al.* [1996], and the grey-filled polygons represent their reported errors.

to have an inverse relationship with energy [*Hammond et al.*, 1996]. Whereas over the common energy range, our results do not demonstrate this trend. This can be seen more clearly in Figure 7, discussed below.

A comparison with previous results of the change in strahl width with radial distance as a function of energy is shown in Figure 7. Our results are shown (black solid line + blue errors) together with the relations derived observationally (red dashed line) by *Hammond et al.* [1996] and via modeling (orange dashed line) by *Owens et al.* [2008]. We fit our results with a linear function using a least squares fit method as previously detailed (black dashed line + black dotted errors). We find that there is a slight increase in strahl pitch angle scattering rate with increasing electron energy. This is in contrast to the results of *Hammond et al.* [1996] and *Owens et al.* [2008], which showed an increase in width with radial distance that monotonically decreased with electron energy. However, it must be noted that observational results obtained by *Hammond et al.* [1996] have a

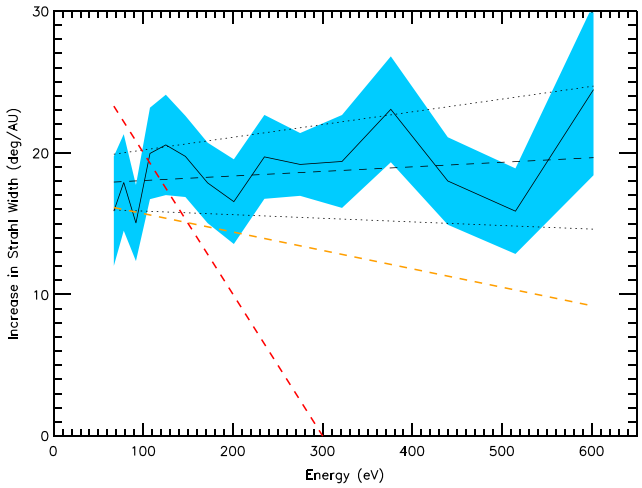

Figure 7. Variation in strahl width per unit distance as a function of electron energy, obtained from the linear fits to the strahl width versus radial distance distributions. The results from this study are represented by the solid black line, and the blue-filled polygon shows the 1σ errors for the linear fits. The red dashed line represents the extrapolated Ulysses results reported by *Hammond et al.* [1996]. The orange dashed line represents the extrapolated *Owens et al.* [2008] results obtained through an empirical model based on the *Hammond et al.* [1996] observations. The black dashed line is a linear fit to the results from this study, and the black dotted line represents the 1σ error for the fit.

significantly steeper decrease with energy than the modeling results obtained by *Owens et al.* [2008]. We discuss the ramifications of this in the following section.

5. Discussion

In this study we present observations of strahl pitch angle width evolution as a function of radial distance and electron energy over radial distances from ~1 to 5.5 AU. We used data obtained by the Cassini spacecraft across its interplanetary voyage to the Kronian system in order to characterize changes in the strahl distributions over a heliocentric radial range that is significantly wider than previously studied [e.g., *Hammond et al.*, 1996]. By using Cassini, we are able to minimize the effects of variable heliospheric latitudes, which has been invoked as a potential influence on electron observations [e.g., *Hammond et al.*, 1996; *Owens et al.*, 2008] or indeed the potential difficulties associated with intercalibration of multiple spacecraft datasets [e.g. *Maksimovic et al.*, 2005].

In order to derive clear strahl signatures using Cassini CAPS ELS, several assumptions were required. Most importantly, we assume that the solar wind can be considered to be made up of a tangled network of fossil flux tubes, which originate in the corona and expand outward with the solar wind flow [e.g., *Borovsky*, 2008; *Neugebauer and Giacalone*, 2015]. Some studies that have argued that these "flux tube boundaries" are more likely to be structures that develop in transit due to turbulence [e.g., *Owens et al.*, 2011]. However, whether the boundary forms in the corona or develops further out into interplanetary space is not critically important for our analysis. We simply use these IMF discontinuities in order to distinguish between regions which have relatively steady electron populations and therefore can support the longer-term averaging needed to derive full pitch angle distributions from Cassini. It should also be noted that identifying IMF discontinuities is not the only method of finding flux tube boundaries and that observed changes in other parameters, such as solar wind bulk velocity [*Borovsky*, 2008] are often used in conjunction with magnetic field information. Since Cassini CAPS has a limited FOV (see section 3), the derivation of accurate solar wind bulk parameters, such as density, temperature, and velocity, is more often than not impossible or else relies heavily on assumptions [e.g., *Paschmann et al.*, 2000; *Rymer*, 2004; *Lewis et al.*, 2008]. Thus, one important aspect not accounted for in this study is the previous observation that strahl pitch angle width is narrower in high speed solar wind streams [e.g., *Feldman et al.*, 1978; *Fitzenreiter et al.*, 1998; *Anderson et al.*, 2012]. As no bulk parameters are routinely available from Cassini, we cannot make any statistical conclusions on the radial dependence of strahl that separate any potential effects of the fast and slow solar wind on the evolution of electron pitch angle distributions.

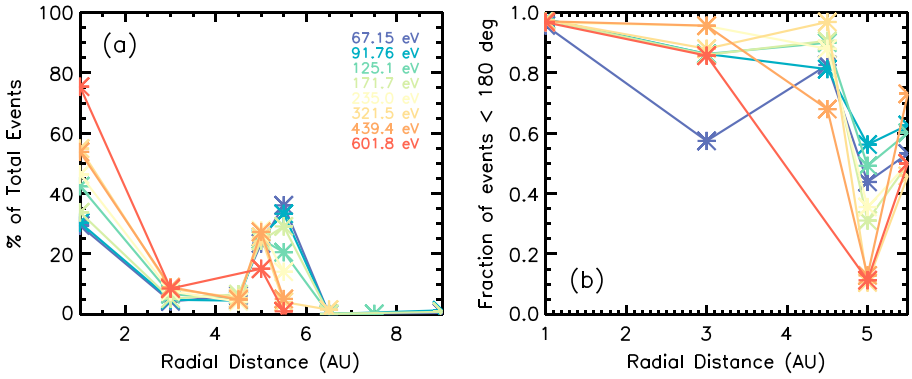

Figure 8. (a) The percentage of total events examined (i.e., that pass the acceptance criteria specified in section 3.2) for each central energy as a function of radial distance. Each energy is represented by a different color ranging from 67.15 eV (purple) to 601.8 eV (red). (b) The fraction of events examined at each radial distance that have a pitch angle width ≤180° and therefore can be considered to be a beam, against radial distance. Each central energy is represented by a the same color as in Figure 8a.

Although our study ranges across 1 to 9 AU, there are very few events beyond 5.5 AU that fulfill our acceptance criteria, as outlined in section 3.2. The events that were considered acceptable for examination because they fulfilled the count rate criteria and the beam-like distribution criteria are shown in Figures 8a and 8b. This can be seen in Figure 8a which shows the percentage of total events examined for each central energy as a function of radial distance. This plot shows that the majority of events examined in this study are near the Earth and Jupiter flybys. It can also be seen that for higher-energy electrons, the percentage of total events examined drops off more rapidly with radial distance, most likely because of low count rates. Figure 8b shows that the fraction of pitch angle distributions examined which have a FWHM <180° also falls with radial distance, e.g., dropping from ~0.95 to 0.60 by 5.5 AU for ~120 eV. Hence, we are only able to derive median strahl pitch angles for ~1–5.5 AU, and thus, we conclude that at larger radial distances, the strahl is most likely completely scattered to form part of the halo population. This is consistent with previous observations of pitch angle width broadening with radial distance from ~ 1 to 2.5 AU [*Hammond et al.*, 1996] and observations of halo to strahl relative number density increasing with radial distance [e.g., *Maksimovic et al.*, 2005; *Štverák et al.*, 2009]. There is a notable decrease in the number of beam-like distributions at 5 AU, which is particularly pronounced for higher electron energies, and suggests that solar wind conditions at this distance may have been favorable for strahl scattering. Further analysis to find estimations of the prevailing solar wind conditions experienced at the time, including a detailed analysis of the magnetic fluctuations observed, may provide some insight into this deviation. The gradual increase of median pitch angle width over a large radial range also has implications regarding the formation of the halo. The implication being that for an approximately isotropic halo to be observed at 0.3 AU [e.g., *Štverák et al.*, 2008] to be solely a result of scattering of a suprathermal beam, much stronger scattering affects would need to be acting closer to the Sun. Extrapolation of linear fits to the data from Figure 4 suggests that by 10 AU, the majority of strahl will have been scattered to pitch angle widths >180°. This implies that indications of strahl found at ~10 AU [*Walsh et al.*, 2013] are more likely to be the result of a halo temperature anisotropy, than any field-aligned electron beam. However, it should be noted that our study is concerned with average strahl behavior, whereas the results obtained at 10 AU were the result of an extended case study. Hence, our findings do not completely discount the possibility that strahl, subjected to fewer scattering events than average, may have been observed at 10 AU during the four day interval considered by *Walsh et al.* [2013].

In general, strahl pitch angle width increases with heliocentric radial distance from ~ 1 to 5.5 AU, in keeping with previous observations of strahl pitch angle width from ~ 1 to 2.5 AU [*Hammond et al.*, 1996]. This implies that strahl is subjected to pitch angle scattering throughout the radial distances that Cassini samples. However, we cannot conclude as to whether scattering is a relatively continuous or intermittent process as, in this paper, we solely investigate general trends of electron evolution. We observe a generally constant pitch angle width increase with distance for each energy, though with significant spread and variation at certain energies (see Figure 4). However, it should be noted that although the IMF is generally well described by the Parker model [e.g., *Burlaga et al.*, 1998; *Forsyth et al.*, 1996], the magnetic field orientation can also deviate significantly [e.g., *Borovsky*, 2010]. This has implications for the consistency of adiabatic focussing experienced

by the electrons, as a more radial (less radial) IMF would result in greater (lesser) narrowing of the strahl beam per unit radial distance, as the change in field strength per unit radial distance is greater for a more radial field [e.g., *Owens et al.*, 2008]. It is also possible that there may be more than one scattering mechanism acting on the electrons with different mechanisms being more dominant at different radial distances, which may also explain the significant variation seen for some of the electron energies shown in Figure 4 after ~ 3 AU.

In this study we observe different energy relations for strahl pitch angle width at different radial distances (see Figure 5). We find that pitch angle width as a function of energy is approximately constant for higher energies at 5 AU and across all energies at 5.5 AU, but that some slight peaks are observed for particular strahl energies at 3 and 5 AU, which may indicate slight preferential scattering for a particular energy. We also find that at both 1 and 4.5 AU, there is a relatively clear decrease in strahl width with energy for lower energies and the increase in strahl width with energy for higher energies. It is important to note that the inherent variability of strahl has resulted in quite large uncertainties in Figure 5. Narrowing pitch angle width with increasing strahl energy has been found by multiple solar wind electron investigations at 1 AU [e.g., *Feldman et al.*, 1978; *Pilipp et al.*, 1987a; *Fitzenreiter et al.*, 1998]. Pitch angle narrowing is thought to be consistent with the theoretical proposal of resonant interaction with whistler mode waves generated via a core electron temperature anisotropy as the strahl pitch angle scattering mechanism [*Saito and Gary*, 2007]. Strahl width that increases with increasing energy has also previously been observed, during periods of enhanced turbulence within the low-frequency whistler regime [*Pagel et al.*, 2007]. An increasing width with energy is theorized to correspond to resonant scattering due to enhancements in the broadband spectra of whistler fluctuations that persist in the solar wind [*Vocks et al.*, 2005; *Saito and Gary*, 2007]. The variation in energy relations observed and the significant uncertainties found suggests that there are multiple scattering mechanisms affecting the strahl population in the solar wind across multiple distances. These mechanisms are likely to produce competing effects on the energy relation of strahl width. This is in line with statistical findings at 1 AU which demonstrated that at any given time, it was equally probable to observe strahl that either broadened or narrowed with electron energy [*Anderson et al.*, 2012].

Previous results have shown that beyond 2.5 AU, there are indications that the increase in strahl width with radial distance falls off, such that at beyond a certain distance, it was expected that strahl width may remain approximately constant [*Hammond et al.*, 1996]. Our results extend out to 5.5 AU and demonstrate that strahl pitch angle widths continue to increase over this entire radial range. We note here that *Hammond et al.* [1996] used Ulysses data over a large heliolatitude range of +30° to −50°. Moreover, as the IMF becomes less tightly wound (more radial) as heliolatitude increases [*Forsyth et al.*, 2002]. Therefore, any change in heliolatitude would affect the adiabatic focussing experienced by strahl electrons [*Owens et al.*, 2008], narrowing the expected strahl widths at higher heliolatitudes. Due to Cassin's near-equatorial trajectory, the observations reported in this study were obtained with minimal latitudinal variation. Hence, the discrepancy between our results and *Hammond et al.* [1996] is likely due to the differing heliolatitude range covered by of the spacecraft.

A direct comparison between previous Ulysses results [*Hammond et al.*, 1996] and the results obtained in this study using Cassini is shown in Figure 6. Our results lie within the errors of previous estimates of strahl pitch angle width evolution, although we note here that previous errors (grey-filled area) are somewhat larger than those calculated within this study. Hence, we believe that we provide a reliable and robust linear relationship between strahl pitch angle width with radial distance over a large (4.5 AU) radial range. As can be seen in see Figure 6, and indeed more clearly in Figure 7 (red dashed line), the results obtained by *Hammond et al.* [1996] show an increase in pitch angle width per unit radial distance that decreased with electron energy. This is in contrast to our results, as we observe the opposite trend, with higher-energy strahl beams broadening slightly more per unit distance than for lower energies. We discuss the implications on the potential scattering mechanism of strahl below.

Figure 6 also shows the increase in strahl width per astronomical unit as a function of energy for the modeled results of *Owens et al.* [2008], based upon empirical fits to data within 2.5 AU presented in *Hammond et al.* [1996]. The increase in strahl pitch angle width with distance obtained by *Owens et al.* [2008], for ~80 eV strahl is approximately the same as the observational results obtained in this study for the same energy, which in turn is of course consistent with the results of *Hammond et al.* [1996]. Extrapolation of the modeled results for ~80 eV to 5 AU gives a strahl pitch angle width of ~100°, which is in agreement with our median strahl pitch angle widths found at this distance using Cassini (~110°). However, at higher energies our observations diverge from the *Owens et al.* [2008] model, as higher-energy strahl broaden significantly more per

astronomical unit than their lower energy counterparts (see Figure 7). It has been demonstrated that the effect of adiabatic focusing in a Parker spiral magnetic field, combined with a constant pitch angle scattering rate (constant with time, radial distance, and electron energy) produces a weak energy dependence for strahl widths with radial distance (as shown in Figure 7 by the orange dashed line) [*Owens et al.*, 2008]. This can be explained by time-of-flight effects, as faster field-aligned electrons traveling outward along a Parker spiral field will experience a larger decrease in magnetic field strength per unit time/distance. Hence, in the presence of a constant pitch angle scattering rate, the effects of adiabatic focussing are stronger for more energetic electrons. Hence, our results suggest that the scattering mechanism has an intrinsic energy relation beyond time-of-flight effects.

It has been hypothesized that resonant scattering due to broadband whistler fluctuations resulting from turbulent cascade can explain why higher-energy strahl is experiencing greater pitch angle broadening [e.g., *Vocks et al.*, 2005; *Saito and Gary*, 2007; *Pagel et al.*, 2007]. It has also been shown that observations of this energy relation occur in conjunction with periods of enhanced magnetic field fluctuations in the whistler frequency range [*Pagel et al.*, 2007] and that whistler-like fluctuations are often observed in the solar wind [e.g., *Lacombe et al.*, 2014]. Hence, our results suggest that although there are multiple strahl scattering mechanisms present in the solar wind, a broadband spectrum of whistler mode waves is likely to play a dominant role in the radial evolution of strahl pitch angle distributions.

It must be noted that we have not considered different solar wind regimes within this study, in which differing whistler mode wave generation mechanisms could potentially be invoked. The slow solar wind is often reported to have a broader strahl pitch angle distribution for a given energy than the fast solar wind [e.g., *Feldman et al.*, 1978; *Fitzenreiter et al.*, 1998; *Anderson et al.*, 2012]. In this study we have also not considered any measurements from within 1 AU, where adiabatic focussing effects are more significant. Further investigation is required in order to establish the rate of strahl pitch angle broadening within 1 AU and also to ascertain if there are differences in the scattering mechanism for the slow and fast solar wind.

6. Conclusions

In this study we have examined Cassini CAPS ELS data from ~1 to 9 AU to significantly extend the heliocentric radial range of strahl electron pitch angle width observations to ~5.5 AU. We find a clear increase in strahl pitch angle width with heliocentric radial distance from 1 to 5.5 AU and conclude that strahl is most likely completely scattered at radial distances beyond 5.5 AU and before 10 AU. Strahl beams are therefore generally unlikely to be observed at large radial distances, unless subjected to significantly lower scattering rates than average. Hence, strahl is more likely to have become scattered to form part of the diffuse halo population and the results obtained by *Walsh et al.* [2013] case study at 10 AU could be explained by either a statistical outlier or a halo temperature anisotropy.

We find that the relationship between strahl pitch angle width and electron energy varies within a given radial distance and at different heliocentric radial distances. It is possible that there are multiple different resonant and non-resonant scattering mechanisms in the solar wind, which have a variable and competitive presence. However, our results also show that whatever processes are competing, there must be an explicit energy dependence in the dominant pitch angle scattering mechanism that accounts for greater pitch angle broadening per unit radial distance for higher-energy electrons. We conclude that resonant scattering due to broadband whistler fluctuations invoked by *Pagel et al.* [2007] and *Saito and Gary* [2007] is the most likely candidate to explain our results.

Further understanding of the heliospheric evolution of strahl electron beams could provide insight into a number of different aspects of solar wind physics, including the origin of suprathermal electrons in the solar corona, the transport of solar wind heat flux, and the topology of the IMF. Our study provides measurements of strahl evolution in the ecliptic plane as a function of energy across the largest possible radial range available to date, providing clear constraints on field-aligned electron dynamics, and the electromagnetic waves that they interact with. Future studies will focus on determining the nature of these wave-particle interactions.

Acknowledgments

G.A.G. is supported by a UCL IMPACT studentship. I.J.R., C.J.O., G.H.J., and A.J.C. are supported by the STFC consolidated grant to MSSL, ST/N000722/1. C.S.A. was supported by a Royal Society Research Fellowship C.F. is supported by NERC IRFNE/N014480/1. We thank the Cassini instrument teams for the provision of the data used in this study, in particular the CAPS ELS and MAG team members at MSSL and ICL, respectively. Data for this study can be found at NASA's Planetary Data System (https://pds.jpl.nasa.gov).

References

Achilleos, N., et al. (2006), Orientation, location, and velocity of Saturn's bow shock: Initial results from the Cassini spacecraft, *J. Geophys. Res.*, *111*, A03201, doi:10.1029/2005JA011297.

Anderson, B. R., R. M. Skoug, J. T. Steinberg, and D. J. McComas (2012), Variability of the solar wind suprathermal electron strahl, *J. Geophys. Res.*, *117*, A04107, doi:10.1029/2011JA017269.

Arridge, C. S., N. Achilleos, M. K. Dougherty, K. K. Khurana, and C. T. Russell (2006), Modeling the size and shape of Saturn's magnetopause with variable dynamic pressure, *J. Geophys. Res.*, *111*, A11227, doi:10.1029/2005JA011574.

Arridge, C. S., L. K. Gilbert, G. R. Lewis, E. C. Sittler, G. H. Jones, D. O. Kataria, A. J. Coates, and D. T. Young (2009), The effect of spacecraft radiation sources on electron moments from the cassini CAPS electron spectrometer, *Planet. Space Sci.*, *57*(7), 854–869, doi:10.1016/j.pss.2009.02.011.

Bale, S. D., M. Pulupa, C. Salem, C. H. K. Chen, and E. Quataert (2013), Electron heat conduction in the solar wind: Transition from Spitzer-Härm to the collisionless limit, *Astrophys. J. Lett.*, *769*(2), L22, doi:10.1088/2041-8205/796/2/L22.

Borovsky, J. E. (2008), Flux tube texture of the solar wind: Strands of the magnetic carpet at 1 AU?, *J. Geophys. Res.*, *113*, A08110, doi:10.1029/2007JA012684.

Borovsky, J. E. (2010), Contribution of strong discontinuities to the power spectrum of the solar wind, *Phys. Rev. Lett.*, *105*, 111102, doi:10.1103/PhysRevLett.105.111102.

Burlaga, L. F., N. F. Ness, Y.-M. Wang, and N. R. Sheeley (1998), Heliospheric magnetic field strength out to 66 AU: Voyager 1, 1978–1996, *J. Geophys. Res.*, *103*(A10), 23,727–23,732, doi:10.1029/98JA01433.

Che, H., and M. L. Goldstein (2014), The origin of non-Maxwellian solar wind electron velocity distribution function: Connection to nanoflares in the solar corona, *Astrophys. J. Lett.*, *795*(2), L38.

de Koning, C. A., J. T. Gosling, R. M. Skoug, and J. T. Steinberg (2006), Widths of suprathermal pitch angle distributions during solar electron bursts: ACE observations, *J. Geophys. Res.*, *111*, A04101, doi:10.1029/2005JA011326.

Dougherty, M., et al. (2004), The Cassini magnetic field investigation, in *The Cassini-Huygens Mission*, edited by M. Dougherty et al., pp. 331–383, Springer, Netherlands, doi:10.1007/978-1-4020-2774-1_4.

Feldman, W. C., J. R. Asbridge, S. J. Bame, M. D. Montgomery, and S. P. Gary (1975), Solar wind electrons, *J. Geophys. Res.*, *80*(31), 4181–4196, doi:10.1029/JA080i031p04181.

Feldman, W. C., J. R. Asbridge, S. J. Bame, J. T. Gosling, and D. S. Lemons (1978), Characteristic electron variations across simple high-speed solar wind streams, *J. Geophys. Res.*, *83*(A11), 5285–5295, doi:10.1029/JA083iA11p05285.

Fitzenreiter, R. J., K. W. Ogilvie, D. J. Chornay, and J. Keller (1998), Observations of electron velocity distribution functions in the solar wind by the wind spacecraft: High angular resolution strahl measurements, *Geophys. Res. Lett.*, *25*, 249–252, doi:10.1029/97GL03703.

Forsyth, R., A. Balogh, T. Horbury, G. Erdös, E. Smith, and M. Burton (1996), The heliospheric magnetic field at solar minimum: Ulysses observations from pole to pole, *Astron. Astrophys.*, *316*, 287–295.

Forsyth, R. J., A. Balogh, and E. J. Smith (2002), The underlying direction of the heliospheric magnetic field through the Ulysses first orbit, *J. Geophys. Res.*, *107*(A11), 1405, doi:10.1029/2001JA005056.

Gosling, J. T., S. J. Bame, W. C. Feldman, D. J. McComas, J. L. Phillips, and B. E. Goldstein (1993), Counterstreaming suprathermal electron events upstream of corotating shocks in the solar wind beyond 2 AU: Ulysses, *Geophys. Res. Lett.*, *20*(21), 2335–2338, doi:10.1029/93GL02489.

Gosling, J. T., D. N. Baker, S. J. Bame, W. C. Feldman, R. D. Zwickl, and E. J. Smith (1987), Bidirectional solar wind electron heat flux events, *J. Geophys. Res.*, *92*(A8), 8519–8535, doi:10.1029/JA092iA08p08519.

Gurgiolo, C., M. L. Goldstein, A. F. Viñas, and A. N. Fazakerley (2012), Direct observations of the formation of the solar wind halo from the strahl, *Ann. Geophys.*, *30*(1), 163–175, doi:10.5194/angeo-30-163-2012.

Hammond, C., W. Feldman, D. McComas, J. Phillips, and R. Forsyth (1996), Variation of electron-strahl width in the high-speed solar wind: Ulysses observations, *Astron. Astrophys.*, *316*, 350–354. provided by the SAO/NASA Astrophysics Data System.

Hu, Y. Q., S. R. Habbal, and X. Li (1999), On the cascade processes of Alfvén waves in the fast solar wind, *J. Geophys. Res.*, *104*(A11), 24,819–24,834, doi:10.1029/1999JA900340.

Lacombe, C., O. Alexandrova, L. Matteini, O. Santolík, N. Cornilleau-Wehrlin, A. Mangeney, Y. de Conchy, and M. Maksimovic (2014), Whistler mode waves and the electron heat flux in the solar wind: Cluster observations, *Astrophys. J.*, *796*(1), 5.

Landi, S., L. Matteini, and F. Pantellini (2012), On the competition between radial expansion and Coulomb collisions in shaping the electron velocity distribution function: Kinetic simulations, *Astrophys. J.*, *760*(2), 143, doi:10.1088/0004-637X/760/2/143.

Lewis, G., N. André, C. Arridge, A. Coates, L. Gilbert, D. Linder, and A. Rymer (2008), Derivation of density and temperature from the Cassini-Huygens CAPS electron spectrometer, *Planet. Space Sci.*, *56*(7), 901–912, doi:10.1016/j.pss.2007.12.017.

Li, B., I. H. Cairns, J. T. Gosling, G. Steward, M. Francis, D. Neudegg, H. Schulte in den Bäumen, P. R. Player, and A. R. Milne (2016), Mapping magnetic field lines between the Sun and Earth, *J. Geophys. Res. Space Physics*, *121*, 925–948, doi:10.1002/2015JA021853.

Lin, R. P. (1998), *Wind observations of suprathermal electrons in the interplanetary medium*,pp. 61–78, Springer, Dordrecht, Netherlands, doi:10.1007/978-94-011-4762-0_4.

Linder, D., A. Coates, R. Woodliffe, C. Alsop, A. Johnstone, M. Grande, A. Preece, B. Narheim, and D. Young (1998), The Cassini CAPS electron spectrometer, in *Measurement Techniques in Space Plasmas: Particles*, edited by R. F. Pfaff, J. E. Borovsky, and D. T. Young, pp. 257–262, AGU, Washington, D. C.

Maksimovic, M., et al. (2005), Radial evolution of the electron distribution functions in the fast solar wind between 0.3 and 1.5 AU, *J. Geophys. Res.*, *110*, A09104, doi:10.1029/2005JA011119.

Markwardt, C. B. (2009), Non-linear least squares fitting in IDL with MPFIT, Proc. ADASS XVIII, ASP Conf. Ser., vol. 411, edited by D. Bohlender, P. Dowler, and D. Durand, p. 251. arXiv preprint arXiv:0902.2850.

Matson, D., L. Spilker, and J.-P. Lebreton (2003), The Cassini/Huygens mission to the Saturnian system, in *The Cassini-Huygens Mission*, edited by D. Matson, L. Spilker, and J.-P. Lebreton, pp. 1–58, Springer, Netherlands, doi:10.1007/978-94-017-3251-2_1.

Neugebauer, M., and J. Giacalone (2015), Energetic particles, tangential discontinuities, and solar flux tubes, *J. Geophys. Res. Space Physics*, *120*, 8281–8287, doi:10.1002/2015JA021632.

Owens, M., R. Wicks, and T. Horbury (2011), Magnetic discontinuities in the near-Earth solar wind: Evidence of in-transit turbulence or remnants of coronal structure?, *Sol. Phys.*, *269*(2), 411–420, doi:10.1007/s11207-010-9695-0.

Owens, M. J., and R. J. Forsyth (2013), The heliospheric magnetic field, *Living Rev. Sol. Phys.*, *10*(5), doi:10.1007/lrsp-2013-5.

Owens, M. J., N. U. Crooker, and N. A. Schwadron (2008), Suprathermal electron evolution in a Parker spiral magnetic field, *J. Geophys. Res.*, *113*, A11104, doi:10.1029/2008JA013294.

Pagel, C., S. P. Gary, C. A. de Koning, R. M. Skoug, and J. T. Steinberg (2007), Scattering of suprathermal electrons in the solar wind: ACE observations, *J. Geophys. Res.*, *112*, A04103, doi:10.1029/2006JA011967.

Paschmann, G., A. N. Fazakerley, and S. J. Schwartz (2000), Moments of plasma velocity distributions, in *Analysis Methods for Multi-Spacecraft Data*, vol. 1, edited by G. Paschmann, and P. W. Daly, pp. 125–157, Int. Space Sci. Inst., Bern.

Pierrard, V., M. Maksimovic, and J. Lemaire (2001), Self-consistent model of solar wind electrons, *J. Geophys. Res.*, *106*(A12), 29,305–29,312, doi:10.1029/2001JA900133.

Pilipp, W. G., H. Miggenrieder, K. H. Mühlhäuser, H. Rosenbauer, R. Schwenn, and F. M. Neubauer (1987a), Variations of electron distribution functions in the solar wind, *J. Geophys. Res.*, *92*(A2), 1103–1118, doi:10.1029/JA092iA02p01103.

Pilipp, W. G., H. Miggenrieder, M. D. Montgomery, K. H. Mühlhäuser, H. Rosenbauer, and R. Schwenn (1987b), Characteristics of electron velocity distribution functions in the solar wind derived from the helios plasma experiment, *J. Geophys. Res.*, *92*(A2), 1075–1092, doi:10.1029/JA092iA02p01075.

Rymer, A. M. (2004), Analysis of Cassini plasma and magnetic field measurements from 1–7 AU, PhD thesis, Univ. of London, Univ. College London (United Kingdom), provided by the SAO/NASA Astrophysics Data System, Harvard Univ., Cambridge, Mass.

Rymer, A. M., A. J. Coates, K. Svenes, G. A. Abel, D. R. Linder, B. Narheim, M. Thomsen, and D. T. Young (2001), Cassini plasma spectrometer electron spectrometer measurements during the Earth swing-by on August 18, 1999, *J. Geophys. Res.*, *106*(A12), 30,177–30,198, doi:10.1029/2001JA900087.

Saito, S., and S. P. Gary (2007), All whistlers are not created equally: Scattering of strahl electrons in the solar wind via particle-in-cell simulations, *Geophys. Res. Lett.*, *34*, L01102, doi:10.1029/2006GL028173.

Scime, E. E., S. J. Bame, W. C. Feldman, S. P. Gary, J. L. Phillips, and A. Balogh (1994), Regulation of the solar wind electron heat flux from 1 to 5 AU: Ulysses observations, *J. Geophys. Res.*, *99*(A12), 23,401–23,410, doi:10.1029/94JA02068.

Smith, H. M., E. Marsch, and P. Helander (2012), Electron transport in the fast solar wind, *Astrophys. J.*, *753*(1), 31.

Štverák, S., P. Trávníček, M. Maksimovic, E. Marsch, A. N. Fazakerley, and E. E. Scime (2008), Electron temperature anisotropy constraints in the solar wind, *J. Geophys. Res.*, *113*, A03103, doi:10.1029/2007JA012733.

Štverák, S., M. Maksimovic, P. M. Trávníček, E. Marsch, A. N. Fazakerley, and E. E. Scime (2009), Radial evolution of nonthermal electron populations in the low-latitude solar wind: Helios, Cluster, and Ulysses observations, *J. Geophys. Res.*, *114*, A05104, doi:10.1029/2008JA013883.

Viñas, A. F., H. K. Wong, and A. J. Klimas (2000), Generation of electron suprathermal tails in the upper solar atmosphere: Implications for coronal heating, *Astrophys. J.*, *528*(1), 509.

Vocks, C., C. Salem, R. P. Lin, and G. Mann (2005), Electron halo and strahl formation in the solar wind by resonant interaction with whistler waves, *Astrophys. J.*, *627*(1), 540.

Walsh, A. P., C. S. Arridge, A. Masters, G. R. Lewis, A. N. Fazakerley, G. H. Jones, C. J. Owen, and A. J. Coates (2013), An indication of the existence of a solar wind strahl at 10 AU, *Geophys. Res. Lett.*, *40*, 2495–2499, doi:10.1002/grl.50529.

Young, D., et al. (1998), Cassini plasma spectrometer investigation, in *Measurement Techniques in Space Plasmas: Particles*, pp. 237–242, AGU, Washington, D. C.

Young, D., et al. (2004), Cassini plasma spectrometer investigation, *Space Sci. Rev.*, *114*(1–4), 1–112, doi:10.1007/s11214-004-1406-4.